

Bis phenylene flattened 13-membered tetraamide macrocyclic ligand (TAML) for square planar cobalt(III)

W. Chadwick Ellis, Alexander D. Ryabov, Andreas Fischer, Joshua A. Hayden, Longzhu Q. Shen, Emile L. Bominaar, Michael P. Hendrich & Terrence J. Collins

To cite this article: W. Chadwick Ellis, Alexander D. Ryabov, Andreas Fischer, Joshua A. Hayden, Longzhu Q. Shen, Emile L. Bominaar, Michael P. Hendrich & Terrence J. Collins (2018): Bis phenylene flattened 13-membered tetraamide macrocyclic ligand (TAML) for square planar cobalt(III), Journal of Coordination Chemistry, DOI: [10.1080/00958972.2018.1487060](https://doi.org/10.1080/00958972.2018.1487060)

To link to this article: <https://doi.org/10.1080/00958972.2018.1487060>



Accepted author version posted online: 11 Jun 2018.



Submit your article to this journal [↗](#)



View related articles [↗](#)



View Crossmark data [↗](#)

Publisher: Taylor & Francis

Journal: *Journal of Coordination Chemistry*

DOI: <http://doi.org/10.1080/00958972.2018.1487060>



Bis phenylene flattened 13-membered tetraamide macrocyclic ligand (TAML) for square planar cobalt(III)¹

W. CHADWICK ELLIS[†], ALEXANDER D. RYABOV^{*†}, ANDREAS FISCHER[‡], JOSHUA A. HAYDEN^{†2}, LONGZHU Q. SHEN^{†3}, EMILE L. BOMINAAR[†], MICHAEL P. HENDRICH[†] and TERRENCE J. COLLINS[†]

[†]Department of Chemistry, Carnegie Mellon University, 4400 Fifth Avenue, Pittsburgh, PA 15213, USA

[‡]Inorganic Chemistry, Department of Chemistry, Royal Institute of Technology, S-100 44 Stockholm, Sweden

The preparation, characterization and evaluation of a cobalt(III) complex

$[\text{Co}\{\overline{(\text{OC})}_2(o,o'\text{-NC}_6\text{H}_4\text{NCO})_2\text{CMe}_2\}(\text{OH}_2)]^-$ with 13-membered tetraamide macrocyclic ligand (TAML) is described. This is a square-planar (X-ray) $S = 1$ paramagnetic (¹H NMR) compound, which becomes an $S = 0$ diamagnetic octahedral species in excess *d*₅-pyridine. Its one-electron oxidation at an electrode is fully reversible with the lowest $E_{1/2}$ value (0.66 V vs SCE) among all investigated Co^{III} TAML complexes. The oxidation results in a neutral blue species which is consistent with a Co^{III}/radical-cation ligand. The ease of oxidation is likely due to the two benzene rings incorporated in the ligand structure (whereas there is just one in many other Co^{III} TAMLs). The oxidized neutral species are unexpectedly EPR silent, presumably due to the π -stacking aggregation. However, they display eight-line hyperfine patterns in the presence of excess of 4-*tert*-butylpyridine or 4-*tert*-butyl isonitrile. The EPR spectra are more consistent with the Co^{III}/radical-cation ligand formulation rather than with a Co^{IV} complex. Attempts to synthesize a similar vanadium complex under the same conditions as for cobalt using $[\text{V}^{\text{VO}}(\text{OCHMe}_2)_3]$ were not successful. TAML-free decavanadate was isolated instead.

Keywords: Macrocyclic complex; TAML; Cobalt; Radical cation; EPR; DFT

*Corresponding author. Email: ryabov@andrew.cmu.edu

¹ Dedicated to Professor Dan Meyerstein on occasion of his 80th birthday, who still enjoys chemistry and keeps his smiling sense of humor!

² Present address: Laboratory Medicine, 525 East 68th Street, Suite F-715, New York, NY 10065, USA

³ Present address: Department of Zoology, University of Cambridge, Downing Street, Cambridge CB2 3EJ, UK

1. Introduction

Tetraamide macrocycle ligand (TAML) system offers a unique environment for transition metal ions and, hence, uncommon polyhedra, oxidation states and coordination numbers of metal complexes [1-3]. Particularly challenging is cobalt chemistry, when the metal in cobalt TAMLs (chart 1) finds itself in the inner cavity of tetra deprotonated amide nitrogens. The oxidation state of cobalt in these square planar complexes is three, *i.e.* both axial coordination sites are vacant. Interestingly, their square planar configuration does not change after 1e oxidation of the cobalt(III) species. Square planar Co^{III} and Co^{IV} complexes are less common than octahedral [4]. Oxidized Co^{III} TAML species are uncharged and therefore soluble in non-polar organic solvents. The first square planar bis(*n*-propylbiuretato)cobaltate(III) complex was crystallographically characterized by Bour *et al.* [5]; Co^{III} was surrounded by four deprotonated amide nitrogens. Collins and Uffelman described the first macrocyclic square planar Co^{III} complex **1** with similar donor centers, which is shown in chart 1 [6]. Similar coordinative polyhedra were later confirmed crystallographically for **2** [7, 8], cyclohexyl variant of **2** [9], **3** [10, 11], **5** [12] and **6** [13]. No X-ray data were however provided for **4**, the polyhedron of which is strongly distorted due to the incorporation of the 2,2'-bipyridine unit in the macrocycle [14].

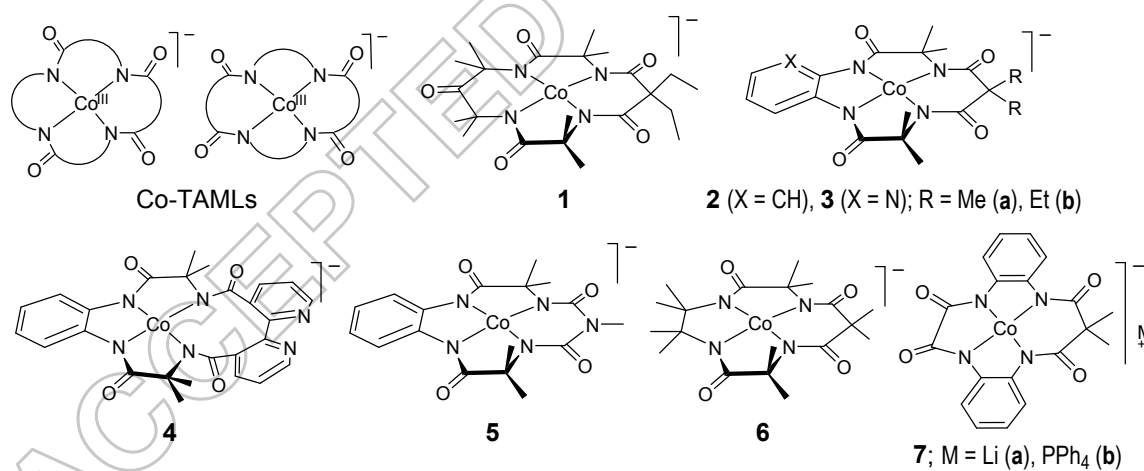


Chart 1. Reported examples of Co^{III} TAMLs **1-6** and new complex **7** described in this work.

The square-planar geometry of both parent Co^{III} and oxidized forms of cobalt TAML complexes makes them attractive as catalysts due to both the open axial coordination sites and the zero charge of the oxidized species. Cobalt TAMLs have been used in the synthesis of

various cyclic carbonates from epoxides and CO₂ with up to 100% yields and turnover frequency (TOF) of 0.1 s⁻¹ [8], in oxygen atom transfer reactions [15] and in the oxidation of water [12, 13]. The reactivity of TAML complexes is controlled by the nature of their ligands [16].⁴

Understandably, new cobalt TAML complexes are potentially viable and herein we describe the synthesis, characterization and some properties of the new cobalt(III) TAML complex **7** which are compared with those of complexes **1-6**. Previously, iron(III) complexes with similar ligands have been reported [18, 19]. They belong to the fourth generation of iron TAML activators of peroxides [20] and are very reactive, in fact the most reactive, in catalytic oxidations by H₂O₂ in the aqueous medium [16]. This noteworthy reactivity of the iron counterparts suggested that it might be worthwhile to revisit cobalt-centered TAMLs by the example of **7**. Though the synthesis of the ligand of **7** and their ring-substituted derivatives was reported earlier [19], we describe additional useful information regarding the preparation of this ligand system.

2. Experimental

2.1. *Materials and methods*

Syntheses were performed under argon with oven dried glassware using Schlenk techniques. Tetrahydrofuran and pyridine were dried and distilled under argon prior to use according to standard laboratory techniques [21]. Other chemicals used were purchased from Sigma Aldrich Chemical or Fisher Scientific and used as received unless stated otherwise. ¹H NMR spectra were recorded on a Bruker Avance™ 300 spectrometer. Chemical shifts in *d*₆-dmsO (δ) are referenced to the residual solvent peak at δ 2.5. Mass spectra (ESI) were obtained using a Thermo-Fisher LCQ ESI/APCI Ion Trap instrument with methanol as a matrix. Elemental analyses were carried out by Midwest Microlabs. Electrochemical measurements were performed on a PC-interfaced potentiostat-galvanostat AUTOLAB PGSTAT 12. A three-electrode setup was used with a glassy carbon working electrode, SCE reference electrode, and auxiliary Pt electrode. Before each measurement, the working electrode was polished with a diamond paste and rinsed with acetone and distilled water.

⁴ Dan Meyerstein was among pioneers who paid special attention to ligand effects on reactivity of metal complexes. More than fifty years ago he reported how ligands influence a speed of redox reactions of cobalt(III) complexes [17].

2.2. EPR Data collection and simulation procedures

X-band (9 GHz) EPR spectra were recorded on a Bruker ESP 300 spectrophotometer with a Bruker bimodal cavity. The modulation amplitude and frequency were 0.5 mT at 100 kHz for all low temperature spectra. Room temperature measurements were done at 300 K. An Oxford ESR 910 cryostat was used for all low temperature measurements and the temperature was calibrated with a carbon glass resistor (Lakeshore CGR-1-1000). A CuEDTA spin standard was used to account for all relevant intensity factors. Simulations of EPR data were performed using the SpinCount software [22].

2.3. Density functional computations

Optimized geometries for cobalt TAML complexes **7**, **13** and **14a,b** were obtained using Becke's three-parameter hybrid functional (B3) [23, 24] along with the Lee–Yang–Parr correlation functional (LYP) [25] and the 6-311G basis set. Spin state $\frac{1}{2}$ and zero charge were assigned to **13** and **14a,b**. Spin state 1 and charge -1 were assigned to **7**. To obtain the simulated structure of **7b**, the cation PPh_4^+ was first placed manually in the vicinity of anion **7** with a reference to the X-ray structural data for **7b**. The constructed complex was then subject to geometry optimization at the DFT level (M06 density functional [26] and triple- ζ basis set 6-311G in the absence of solvent using the Gaussian 09 computational package [27]. A stable structure was obtained upon convergence to the default criteria set in Gaussian. The overlaid X-ray and DFT structures revealed the root mean square difference of 0.36 Å, suggesting minute variation between them.

2.4. Metalation of **10** by cobalt(II) chloride to form **7a**

Tetraamide **10** [19] (100 mg, 366 μmol) was mixed with dry THF (50 mL) in a round bottom flask under argon followed by addition of 4.4 equivalents of lithium bis(trimethylsilyl)amide (1.22 mL of 1 M solution in THF). The mixture was stirred for *ca.* 5 min to obtain a homogeneous solution. Then CoCl_2 (43.3 mg, 334 μmol) was added and the reaction mixture slowly turned dark blue to purple. After stirring overnight, the mixture was opened to air for 15 min. The solid formed was placed on a short silica gel column. The product turned yellow on the silica. Elution by acetone yielded a dark blue to purple solution. The solvent was evaporated to dryness to yield a solid of the same color in 25% yield. An additional portion of **7a**, though of

lower purity, could be precipitated by pouring the THF filtrate (50 mL) into *n*-hexane (250 mL) and recovered by filtration. ESI-MS negative mode (421 m/z).

2.5. Metathesis of 7a to 7b

Complex **7a** (5 mg, 0.01 mmol) was dissolved in a minimum amount of water (*ca.* 2 mL) to yield a yellowish green solution, which was filtered through a 0.25 μm syringe filter. Then PPh_4Cl (40 mg, 0.1 mmol) dissolved in 2 mL H_2O was added dropwise to yield a purple precipitate. This was collected by filtration, rinsed with water, and recrystallized from ethanol/heptane as small pentagonal X-ray quality crystals. Mp 209-211 $^\circ\text{C}$. ^1H NMR (CD_3CN): 27.95(s, 2H, ArH), 25.0(s, 2H, ArH), 7.2(s, 6H, CH_3), 6.1(s, 2H, ArH), 0.2(s, 2H, ArH); 7.4–8.0(m, 20H, Ph). ESI-MS (m/z) negative mode: 421 (**7** anion); positive mode: 339 (PPh_4 cation). Anal. Calcd. for $\text{C}_{43}\text{H}_{34}\text{N}_4\text{O}_4\text{PCo}$: C, 67.90; H, 4.51; N, 7.37. Found: C, 68.30; H, 4.82; N, 7.29%.

2.6. Single-crystal X-ray characterization

Single crystals of **7b** were obtained from ethanol/heptane. $\text{C}_{43}\text{H}_{34}\text{CoN}_4\text{O}_4\text{P}$, $M_r = 760.7$, monoclinic, $P2_1/c$, red, $a = 11.184$ (2) \AA , $b = 10.9653$ (3) \AA , $c = 28.742$ (3) \AA , $\beta = 96.469$ (10) $^\circ$, $T = 299$ K, $Z = 4$, $R_1 = 0.048$, $wR_2 = 0.102$, GOF = 1.02. Data collection was on a Bruker-Nonius KappaCCD (Mo $K\alpha$ radiation), structure solution with direct methods, structure refinement on F^2 with anisotropic thermal parameters for all non-H atoms. H atoms were placed at calculated positions and refined using a riding model.

2.7. Oxidation of 7 to a neutral species

Purple **7a** (1 mg) was placed into a mortar and an excess of $(\text{NH}_4)_2\text{Ce}^{\text{IV}}(\text{NO}_3)_6$ (5 mg) was added. Neither of these compounds is soluble in dichloromethane, benzene, or toluene.

Dichloromethane (1.5 mL dried over MgSO_4) was added to the mortar, and the heterogeneous mixture was ground together under the solvent using a pestle. The solvent quickly turns deep blue (λ_{max} at 860 nm and slightly lesser peak at 700 nm), indicating the formation and dissolution of neutral **13**. When this color maximized, half of the solution was filtered through glass wool into an EPR tube and frozen. The same is done to the other half, except 4-*t*-Bu-pyridine was added to the EPR tube yielding a yellow/orange solution which was then frozen. Reaction yields

were difficult to estimate due to the heterogeneous nature of the reaction and difficulty of isolation of the highly oxidizing product.

2.8. Oxidation of 7 by Br₂

Complex **7a** (1 mg) was dissolved in 1 mL water followed by addition of dichloromethane (1.5 mL) and a drop of bromine water (0.1 mL Br₂ in 1 mL water). The mixture was shaken vigorously until the organic layer was blue. The organic layer was pipetted off and dried over MgSO₄. The blue color was lost slowly and began turning green.

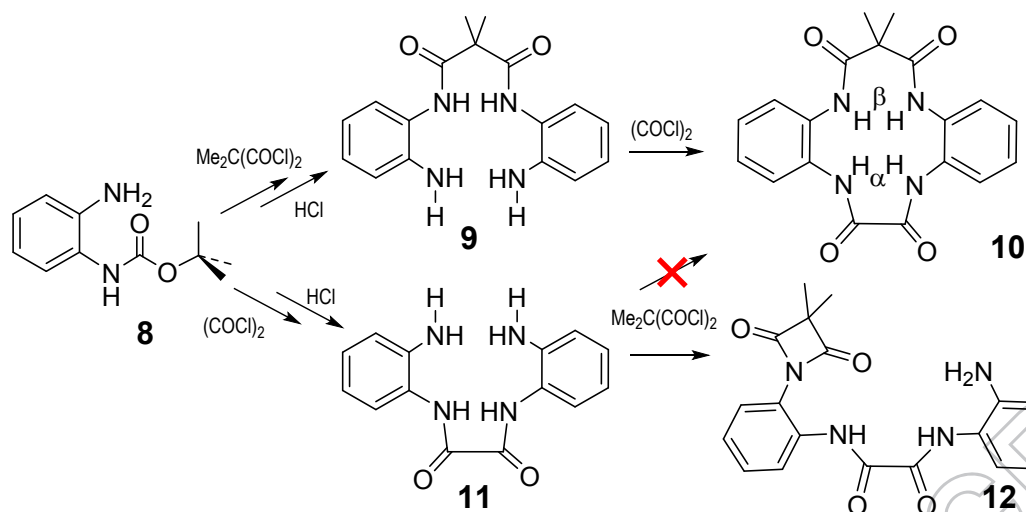
2.9. Attempted metalation of 10 by vanadium(V)

Macrocyclic **10** (50 mg, 0.136 mmol) was placed into a 50 mL dried round bottom flask under argon. Distilled THF (25 mL) was added. Lithium bis(trimethylsilyl) amide (0.2 mL, 1 M in THF, 0.2 mmol) was added (0.367 eq relative to amide protons). Vanadium(V) triisopropoxide oxide (40 mg, 0.164 mmol) was added and stirred. After 24 h, the reaction mixture was poured into 100 mL heptane, and over the course of a few hours, a green solid precipitate formed on the walls of the beaker as heptane evaporated. This was collected (approximately 5 mg), dissolved in water, precipitated with tetraphenylphosphonium chloride, and collected by filtration on filter paper. The precipitate was then dissolved in 2 mL MeCN and 1.5 mL water was added. This mixture was heated at 70 °C in a water bath until approximately 0.5 mL of solvent evaporated, and then left to stand for 2 weeks at room temperature. Small yellow/green crystals that formed were studied by X-ray crystallography [28].

3. Results and discussion

3.1. Comments of the ligand synthesis

An important step in the ligand synthesis is the condensation of two molecules of semi-protected 1,2-diaminobenzene **8** with dimethyl malonyl dichloride to form **9**, which after deprotection with HCl undergoes macrocyclization into **10** reacting with oxalyl dichloride [19] (scheme 1). In principle, a similar result could be achieved through the macrocyclization of **11** (produced from **8** and oxalyl dichloride) with dimethyl malonyl dichloride.



Scheme 1. Two possible syntheses of **10** macrocycle of which the **8** \rightarrow **9** \rightarrow **10** sequence is effective.

Searching for improving the yield of **10** (its overall yield via the **8** \rightarrow **9** \rightarrow **10** sequence was 24% [19]), we have also explored the **8** \rightarrow **11** \rightarrow **10** sequence with a negative result. The macrocyclization of **11** to form **10** did not occur and the imide **12** was produced instead according to the ^1H NMR data. This was rather unexpected because dialkyl malonyl dichloride has previously been used for the macrocyclization of the ligands of complexes **1-3** [8, 29, 30] and **6** [16]. Compounds such as **12** were also observed in the attempted macrocyclization to form ligands of **2** using dimethyl malonyl dichloride in the presence of very strong bases [31]. As another example, using dimethyl malonyl dichloride to couple two equivalents of *o*-nitroaniline resulted in the imide when triethylamine was used, while the coupled product formed when pyridine was the base. In this case, weaker bases did promote the formation of the nitro-derivative of **9**.

To find out why **9** and **11** differed so much in their reactivity towards macrocyclization, theoretical studies were undertaken for **11**. First, the energy of the latter was analyzed as a function of the torsion angle at the oxalamide C–C bond, which was varied from 0.87 to 359.13°. The transoid conformation of **11** with the torsion angle of 180° was by *ca.* 71 kJ mol⁻¹, more energetically advantageous than the cisoid conformation with the torsion angle of 0°. As a result, the two free amino groups of transoid **11** are too far away from each other making it very

problematic for dimethylmalonyl dichloride to "find" them to form macrocycle **10** as opposed to forming imide **12**.

Further, a separation between the free amino groups sufficient for the macrocyclization of **11** was investigated as a function of the same torsion angle. Our data suggest that the angle optimal for the macrocyclization lies in the range from -55 to $+55^\circ$. When the absolute value of the torsion angle is outside this range, the macrocyclization becomes unlikely. Compound **9** lacks the transoid stability of **11** and thus can attain an optimal conformation for macrocyclization via reaction with oxalyl chloride.

3.2. Metalation of **10**

The standard procedure for metalation of TAMLs has been applied for **10**. The ligand was first treated with a strong base (lithium bis(trimethylsilyl)amide) in THF followed by reacting the deprotonated form with cobalt(II) chloride. Exposure of the reaction mixture to air resulted in the formation of the cobalt(III) derivative isolated as a lithium salt **7a**. The higher oxidation state $3+$ is effectively stabilized by four negatively charged deprotonated amide donor centers and **7a** is very stable in the air. Compound **7a** is poorly soluble in organic solvents and therefore the tetraphenylphosphonium salt **7b** was prepared via cation metathesis.

The ease of metalation of **10** encouraged us to make the corresponding TAML complex of vanadium, which was never reported previously [2]. Thus, $[\text{V}^{\text{VO}}(\text{OCHMe}_2)_3]$ was reacted with **10** in THF in the presence of lithium bis(trimethylsilyl)amide. The product, the structure of which was established by X-ray crystallography [28], did not contain **10** and turned out to be an anionic decavanadate (figure 1), presumably $\text{V}_{10}\text{O}_{28}^{6-}$ as characterized, for example, by Evans [32]. It is worth noting that decavanadates are intensively studied due their activity in biological systems [33, 34].

3.3. X-ray Structural and DFT studies of **7b**

The crystal of **7b** suitable for an X-ray study was grown from ethanol/heptane. The structural data have been preliminarily reported elsewhere [28]. The central metal is surrounded by four deprotonated amide nitrogens (figure 2a), which are located in the apices of the square with cobalt sitting in the center. The coordination of Co^{III} by **10** makes the entire complex almost perfectly planar and only the Co-containing six-membered ring exhibits minor distortion; C16

and C19 deviate slightly above and below the four nitrogen planes, respectively. The Co–N bond lengths are 1.816–1.844 Å. The two within the five-membered ring (1.816 and 1.824 Å) are slightly shorter than those of the six-membered ring (1.835 and 1.844 Å). Inverse sequence could be anticipated because N3 and N4 should be more electron-donating due to two methyl groups attached to C16.

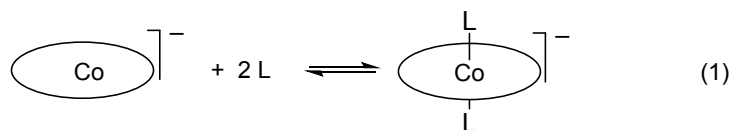
Counter ions are usually not shown for transition metal cations or anions but PPh_4^+ of **7b** is included in figure 2a. The reason is that three phenyl rings could be compared with three piano stool legs leaning on the imaginary plane of the anion. Though the Co \cdots P separation is large (5.335 Å), some atoms of the cation approach rather close to those of the transition metal anion. For example, the C9 \cdots C29 and C2 \cdots C36 separations of 3.227 and 3.668 Å, respectively, may be indicative of π -stacking interactions between phenyl rings of the cation and the anion of **7b**. It is worth noting that the DFT optimization of **7b** ended up in a quite remarkable similarity of the experimental and theoretical portraits (figure 2b). The similarity spreads even on the phosphonium counterion with its closest separations with the anion of 3.406 and 3.604 Å.

3.4. ^1H NMR spectra of free ligand **10** and cobalt(III) complex **7b**

The spectrum of **10** is simple reflecting the existence of the symmetry plane. The amide hydrogens appear as two broadened singlets at δ 9.56 and 9.66 in d_6 -dmsO. Presumably the former arises from the H^β hydrogens of **10** (scheme 1) because of the electron donating effect from the adjacent methyl groups. The methyl groups resonate as one singlet at δ 1.55 at room temperature suggesting a dynamic behavior of **10** in solution. The spectrum of **7b** in d_3 -acetonitrile (figure 3) reveals paramagnetism of the $S = 1$ complex typical of other square planar Co^{III} compounds of this family [7, 9, 35]. All resonances of **7b** cover the δ range from –22 to 8 and only the signals from tetraphenylphosphonium cation are not paramagnetically shifted. The methyl groups appear as one singlet at δ –7.3. Two of the four aromatic hydrogens are stronger shifted to the higher field (δ –27.9 and –25.0) as compared with those at δ –6.2 and –0.1.

The ^1H NMR spectrum of **7b** in less coordinating CDCl_3 solvent is noticeably broader than that in CD_3CN though chemical shifts of the anionic part of the complex do not change. The counter-cation PPh_4^+ , however, reveals itself at δ 4.5–5.5 which is presumably due some ion-pairing between the diamagnetic cation and the paramagnetic anion similar to that observed in the

solid state (see figure 2). The paramagnetic character of the spectrum of **7b** in CDCl₃ practically vanishes on addition of excess *d*₅-py (*ca.* 0.06 mL), which is also accompanied by color change from green to yellow (figure 4). A sharp singlet from the two methyl groups at δ 0.0 is indicative of the octahedral composition of the C_{2v} product formed in accord to eq. 1. A new spectral pattern shown in figure 4 suggests a spin change from *S* = 1 to *S* = 0 on axial coordination of two pyridine ligands.



3.5. Electrochemistry of **7b**

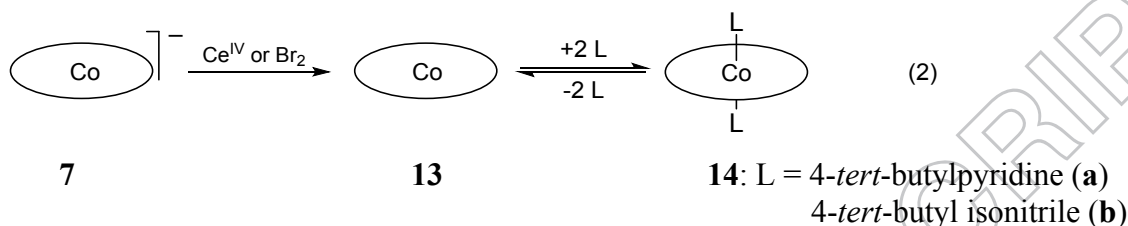
Cyclic voltammograms of **7b** obtained in acetonitrile at scan rates of 50–200 mV s⁻¹ show a Nernstian behavior at the electrode (figure 5). There is a separation between anodic and cathodic peaks of *ca.* 60 mV which is unaffected by the scan rate and consistent with a reversible 1e transfer [36]. It is tempting to formally assign this feature observed at 0.66 V vs SCE to the Co^{IV}/Co^{III} transition but it might be misleading considering the data in table 1 which collects similar information for related Co^{III} TAML complexes. The key question here, which has been raised before [7, 29], is whether this is metal- or ligand-centered oxidation. We believe that the electrochemical data presented here supports the ligand-based model.

First, the electrochemical oxidation at *ca.* 0.8-1.0 V vs SCE is observed clearly when the TAML of Co^{III} complex contains a benzene unit. No oxidation was reported for **1**, which is an arene-free species, for the "switch" complex **3b**, in which benzene ring is replaced by the pyridine fragment, and for the 'beheaded' [38, 39] complex **6** (table 1). Second, the value of *E*_{1/2} for **7b** with two benzene rings is much lower than that for all other complexes in table 1, which have just one ring.

3.6. Oxidation of **7** by Ce^{IV} and Br₂ and EPR studies of the Co^{IV} complexes produced

The value of *E*_{1/2} for **7b** obtained by cyclic voltammetry suggests that strong oxidants should readily convert monoanionic cobalt(III) species **7** into the corresponding neutral derivatives. This happens under the action of cerium(IV) or dibromine. Complex **7a** was oxidized by [NH₄]₂[Ce^{IV}(NO₃)₆] in a slurry using benzene or CH₂Cl₂ where both the reductant and oxidant

are insoluble (eq. 2). Upon oxidation, the neutral complex formed dissolves in the solvent resulting in its color change from colorless to bright blue, which is typical of oxidized square planar TAML complexes of cobalt [7, 9]. The solution was then filtered and the filtrate was used for EPR measurements.



The oxidation of **7** by Br₂ in a 1:1 (v/v) water-CH₂Cl₂ mixture (eq. 2) looks spectacular. Charged **7a** is insoluble in non-polar organic solvents and therefore the aqueous layer is purple. Addition of a trace of Br₂ to the binary mixture followed by its vigorous shaking moves the colored species into the organic phase, which turns bright sky blue due to the formation of the neutral product. The aqueous layer becomes colorless indicative of a quantitative oxidation of **7a**.

The neutral complex **13** is EPR silent, presumably due to aggregation upon freezing which provides anti-ferromagnetic interactions. The aggregation does not occur in the presence of excess *N*- or *C*-ligand, *viz.* 4-*tert*-butylpyridine and 4-*tert*-butyl isonitrile, respectively (eq. 2), which were added prior to freezing. The EPR spectra of **14a,b** are shown in figure 6. The spectra display ⁵⁹Co (*I* = 7/2) eight-line hyperfine patterns at low temperature with *a* = 5.2 and 4.1 mT for **14a,b**, respectively; for **14a** thawed at room temperature, *a* = 2.2 mT. The spectra in figure 6 were simulated using *g* = (1.990, 2.008, 2.004) for **14a**, *g* = (1.998, 2.002, 2.006) for **14b**; and axial hyperfine tensors *A* = (15, 15 147) MHz for **14a** and *A* = (9, 9, 115) MHz for **14b**. The low temperature isotropic values of *g* (2.000) and *A* (59 MHz) for **14a** agree with those obtained from simulation of the room temperature data. The EPR data presented above indicate *S* = 1/2 for both **14a** and **14b**. Furthermore, the very low isotropic value for *A* and isotropic value *g* of 2.00 indicate that the unpaired electron is primarily ligand centered. Therefore, the EPR data confirm a Co^{III}-ligand radical electronic configuration for the 1 electron oxidized state of both complexes.

3.7. DFT Analysis of **7** and **13/14**

A goal of the computational work was to gain theoretical support for the cobalt(III)-ligand radical-cation formulation of the neutral species **13/14**, the experimental evidence for which was deduced from the electrochemical and EPR data. An obstacle here is that the electrochemical data report on the $\mathbf{7} \rightleftharpoons \mathbf{13}$ redox feature but neutral, square-planar **13** did not yield an EPR signal. Instead, it is octahedral **14** that is a source of relevant information.

The orbital energy diagram for square-planar anion **7** is shown in figure 7A. It differs noticeably from idealized square-planar complexes due to π interactions with four *N*-donors which raise the energy of the d_{xz} and d_{yz} orbitals. The d_{z^2} orbital becomes the lowest. The net result is that d^6 **7** is $S = 1$ high spin as illustrated by its paramagnetism (as observed by ^1H NMR), which practically vanishes on addition of excess of pyridine ligand. The square-planar species turns into octahedral as in eq. 1, the energy of the d_{z^2} orbital increases expectedly making the complex low spin ($S = 0$) (figure 7B) as observed by ^1H NMR.

The primary product of 1e oxidation of **7** is **13**, and one might assume that its *d* orbital diagram would match that of **7** (figure 7A) with one fewer electron. However, provided the electron is removed from the ligand and not from the metal, it is hypothesized that the metal retains its $S = 1$ configuration with an antiferromagnetically coupled electron residing in a delocalized fashion across the ligand as in figure 7C. This diagram for a square-planar species corresponds to the cobalt(III)/radical cation ligand. While direct theoretical modeling of the case in figure 7C is problematic due to the lack of relevant EPR data for **13**, the electrochemical behavior in combination with the color and solubility changes seem to be rather convincing.

The model such as in figure 7C, which is consistent with the cobalt(III)/radical cation formulation, could be built for octahedral species **14** (figure 7D). In this case, just as in the reduced state, the axial ligands boost the energy of the d_{z^2} orbital thereby reducing the spin on the metal to $S = 0$ while leaving the ligand radical character intact. It should be taken into account that axial ligands, which raise the energy of the d_{z^2} orbital, are added after the electron transfer. Hence, it could be inferred that the electronic assignment for square-planar **13** is similar and shows that one electron oxidation of cobalt(III) TAMLs is strongly favored by the presence of benzene rings in the ligand system (table 1).

4. Conclusion

The TAML ligand **10**, due to its symmetry, provides interesting insight into the synthesis of macrocycles regarding the nature of synthetic route to be used, which in this case involved final macrocyclization by oxalyl dichloride (scheme 1). The ease of one electron oxidation of **7** compared to all previously reported Co^{III} TAMLs containing a benzene ring in the ligand structure forces one to think that a radical-cation ligand is formed with the oxidation state of cobalt unchanged. Theoretical evidence for this was obtained only for the octahedral product of 1e oxidation **14** generated *after* formation of neutral species **14**. The experimental data are consistent with a ligand centered radical for both species. The ¹H NMR data for **7** obtained in the absence and in the presence of excess of *d*₅-pyridine indicates the $S = 1 \rightarrow S = 0$ spin transition on going from square-planar to octahedral species (eq. 1), which suggests that a similar phenomenon could occur in the oxidized states of **13** and **14**.

Supplementary material

Cif and checkcif files for **7b**.

Acknowledgements

NMR instrumentation at CMU was partially supported by NSF (CHE-0130903 and CHE-1039870). M. P. H. thanks the National Institutes of Health GM49970 for funding. The EPR spectrometer was funded with NSF CHE1126268.

Disclosure statement

No potential conflict of interest was reported by the authors.

Funding

Operating support is acknowledged from the Heinz Endowments (T.J.C.), the Institute for Green Science (T.J.C.), and the Environmental Protection Agency (grant RD 83 to T.J.C.).

References

- [1] A. Chanda, D.-L. Popescu, F. Tiago de Oliveira, E.L. Bominaar, A.D. Ryabov, E. Münck, T.J. Collins. *J. Inorg. Biochem.*, **100**, 606 (2006).

- [2] D.-L. Popescu, A. Chanda, M. Stadler, F. Tiago de Oliveira, A.D. Ryabov, E.L. Bominaar, E. Münck, T.J. Collins. *Coord. Chem. Rev.*, **252**, 2050 (2008).
- [3] T.J. Collins, A.D. Ryabov. *Chem. Rev.*, **117**, 9140 (2017).
- [4] P.V. Bernhardt, G.A. Lawrance. In *Compr. Coord. Chem. II*, J.A. McCleverty, T.J. Meyer (Eds.), pp. 1-145. Elsevier Ltd., Oxford, UK (2004).
- [5] J.J. Bour, P.T. Beurskens, J.J. Steggarda. *J. Chem. Soc., Chem. Commun.*, 221 (1972).
- [6] T.J. Collins, E.S. Uffelman. *Angew. Chem., Int. Ed. Engl.*, **28**, 1509 (1989).
- [7] T.J. Collins, R.D. Powell, C. Slebodnick, E.S. Uffelman. *J. Am. Chem. Soc.*, **113**, 8419 (1991).
- [8] A. Ghosh, P. Ramidi, S. Pulla, S.Z. Sullivan, S.L. Collom, Y. Gartia, P. Munshi, A.S. Biris, B.C. Noll, B.C. Berry. *Catal. Lett.*, **137**, 1 (2010).
- [9] R.E. Patterson, S.W. Gordon-Wylie, C.G. Woomer, R.E. Norman, S.T. Weintraub, C.P. Horwitz, T.J. Collins. *Inorg. Chem.*, **37**, 4748 (1998).
- [10] S.W. Gordon-Wylie, *High valent manganese and cobalt complexes of oxidatively robust N and O donor ligands*, PhD Thesis. Carnegie Mellon University, Pittsburgh (1995).
- [11] C.P. Horwitz, S.W. Gordon-Wylie, Y. Leychkis, D.M. Flynn, S.T. Weintraub, G.R. Clark, T.J. Collins. *J. Phys. Chem. B*, **105**, 8821 (2001).
- [12] D. Das, S. Pattanayak, K.K. Singh, G.S. Sen, B. Garai. *Chem. Commun.*, **52**, 11787 (2016).
- [13] H.-Y. Du, S.-C. Chen, X.-J. Su, L. Jiao, M.-T. Zhang. *J. Am. Chem. Soc.*, 10.1021/jacs.1028b00032 (2018).
- [14] R.O. Saavedra Diaz, R. Le Lagadec, L.Q. Shen, A.D. Ryabov. *J. Coord. Chem.*, **67**, 3909 (2014).
- [15] S. Hong, F.F. Pfaff, E. Kwon, Y. Wang, M.-S. Seo, E. Bill, K. Ray, W. Nam. *Angew. Chem., Int. Ed.*, **53**, 10403 (2014).
- [16] M.A. DeNardo, M.R. Mills, A.D. Ryabov, T.J. Collins. *J. Am. Chem. Soc.*, **138**, 2933 (2016).
- [17] M. Anbar, D. Meyerstein. *Nature*, **206**, 818 (1965).
- [18] W.C. Ellis, C.T. Tran, M.A. Denardo, A. Fischer, A.D. Ryabov, T.J. Collins. *J. Am. Chem. Soc.* 131, 18052-18053 (2009).

- [19] W.C. Ellis, C.T. Tran, R. Roy, M. Rusten, A. Fischer, A.D. Ryabov, B. Blumberg, T.J. Collins. *J. Am. Chem. Soc.*, **132**, 9774 (2010).
- [20] G. Warner, M. Mills, C. Enslin, S. Pattanayak, C. Panda, S. Sen Gupta, A.D. Ryabov, T.J. Collins. *Chem. Eur. J.*, **21**, 6226 (2015).
- [21] W.L.F. Armarego, C.L.L. Chai, *Purification of laboratory chemicals*, Elsevier, USA (2003).
- [22] D.T. Petasis, M.P. Hendrich. *Methods Enzymol.*, **563**, 171 (2015).
- [23] A.D. Becke. *J. Chem. Phys.*, **98**, 5648 (1993).
- [24] A.D. Becke. *J. Chem. Phys.*, **109**, 2092 (1998).
- [25] C. Lee, W. Yang, R.G. Parr. *Phys. Rev. B*, **37**, 785 (1988).
- [26] Y. Zhao, D.G. Truhlar. *Theor. Chem. Acc.*, **120**, 215 (2008).
- [27] M.J. Frisch, G.W. Trucks, H.B. Schlegel, G.E. Scuseria, M.A. Robb, J.R. Cheeseman, G. Scalmani, V. Barone, B. Mennucci, G.A. Petersson, H. Nakatsuji, M. Caricato, X. Li, H.P. Hratchian, A.F. Izmaylov, J. Bloino, G. Zheng, J.L. Sonnenberg, M. Hada, M. Ehara, K. Toyota, R. Fukuda, J. Hasegawa, M. Ishida, T. Nakajima, Y. Honda, O. Kitao, H. Nakai, T. Vreven, J.A. Montgomery, J.E. Peralta, F. Ogliaro, M. Bearpark, J.J. Heyd, E. Brothers, K.N. Kudin, V.N. Staroverov, R. Kobayashi, J. Normand, K. Raghavachari, A. Rendell, J.C. Burant, S.S. Iyengar, J. Tomasi, M. Cossi, N. Rega, J.M. Millam, M. Klene, J.E. Knox, J.B. Cross, V. Bakken, C. Adamo, J. Jaramillo, R. Gomperts, R.E. Stratmann, O. Yazyev, A.J. Austin, R. Cammi, C. Pomelli, J.W. Ochterski, R.L. Martin, K. Morokuma, V.G. Zakrzewski, G.A. Voth, P. Salvador, J.J. Dannenberg, S. Dapprich, A.D. Daniels, O. Farkas, J.B. Foresman, J.V. Ortiz, J. Cioslowski, D.J. Fox. In *Gaussian 09, Revision D.01*, Gaussian, Inc., Wallingford, CT (2009).
- [28] W.C. Ellis, *Green design, synthesis, characterization, and application of a novel family of Fe(III)-TAML peroxide activating homogeneous catalysis*. PhD Thesis, Carnegie Mellon University, Pittsburgh (2010).
- [29] T.J. Collins. *Acc. Chem. Res.*, **27**, 279 (1994).
- [30] T.J. Collins. *Acc. Chem. Res.*, **35**, 782 (2002).
- [31] A. Ghosh, *Design, synthesis and mechanistic studies of iron-TAML catalytic activators of hydrogen peroxide and a new activation chemistry of dioxygen by iron*, PhD Thesis, Carnegie Mellon University, Pittsburgh (2004).

- [32] H.T. Evans, Jr. *Inorg. Chem.*, **5**, 967 (1966).
- [33] M.P.M. Marques, D. Gianolio, S. Ramos, L.A.E. Batista de Carvalho, M. Aureliano. *Inorg. Chem.*, **56**, 10893 (2017).
- [34] M. Aureliano, C.A. Ohlin. *J. Inorg. Biochem.*, **137**, 123 (2014).
- [35] J.C. Brewer, T.J. Collins, M.R. Smith, B.D. Santarsiero. *J. Am. Chem. Soc.*, **110**, 423 (1988).
- [36] A.J. Bard, L.R. Faulkner, *Electrochemical Methods. Fundamentals and Applications*, John Wiley & Sons, New York (1980).
- [37] E.S. Uffelman, *Design, synthesis, and structure of a macrocyclic tetraamide that stabilizes high-valent middle and later transition metals*, PhD Thesis, California Institute of Technology, Pasadena (1992).
- [38] M.R. Mills, L.Q. Shen, D.Z. Zhang, A.D. Ryabov, T.J. Collins. *Inorg. Chem.*, **56**, 10226 (2017).
- [39] M.R. Mills, A.C. Weitz, D.Z. Zhang, M.P. Hendrich, A.D. Ryabov, T.J. Collins. *Inorg. Chem.*, **55**, 12263 (2016).
- [40] L.Q. Shen, *Experimental and theoretical studies of TAML[®] activators : pharmaceuticals degradation, nuclear tunneling and electronic structure analysis*, PhD Thesis, Carnegie Mellon University, Pittsburgh (2013).

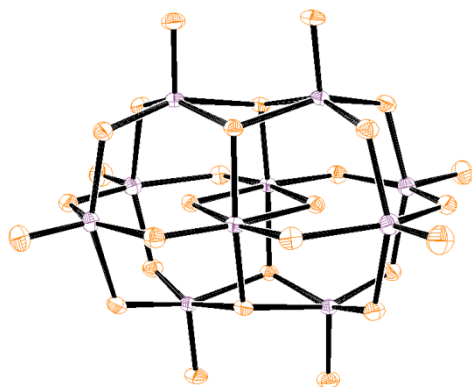


Figure 1. Structure of decavanadate produced by attempted metalation of **10** by $[\text{V}^{\text{VO}}(\text{OCHMe}_2)_3]$ (see text for details) [28].

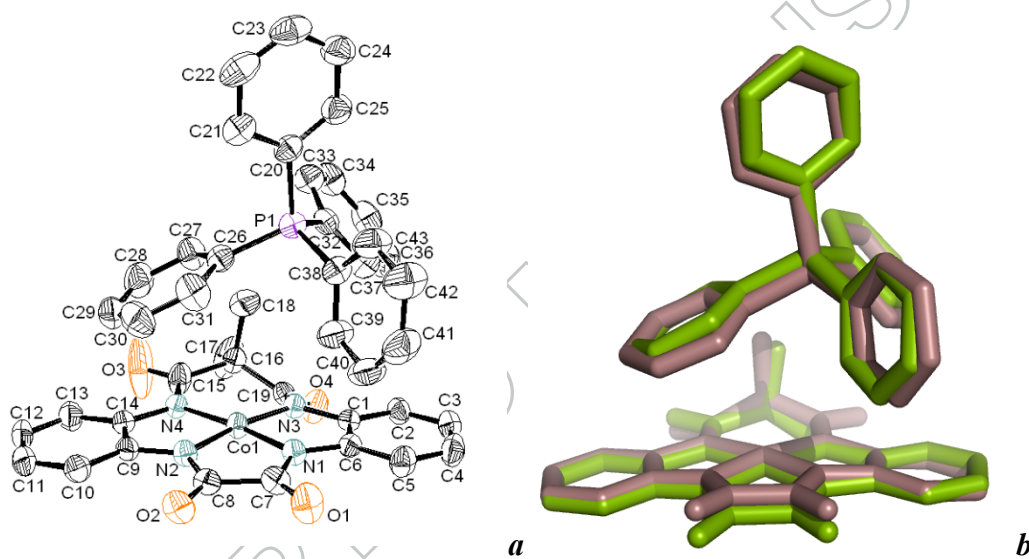


Figure 2. Structure of **7b** elucidated by X-ray crystallography (*a*) and its overlay with a model created by DFT (*b*). Displacement ellipsoids in *a* are drawn at the 50% probability level. Hydrogens are omitted for clarity. Selected bond lengths (in Å): Co–N(1) 1.824(2), Co–N(2) 1.816(2), Co–N(3) 1.835(3), Co–N(4) 1.844(2). DIAMOND release 3.1e, Crystal Impact GbR, Bonn, Germany.

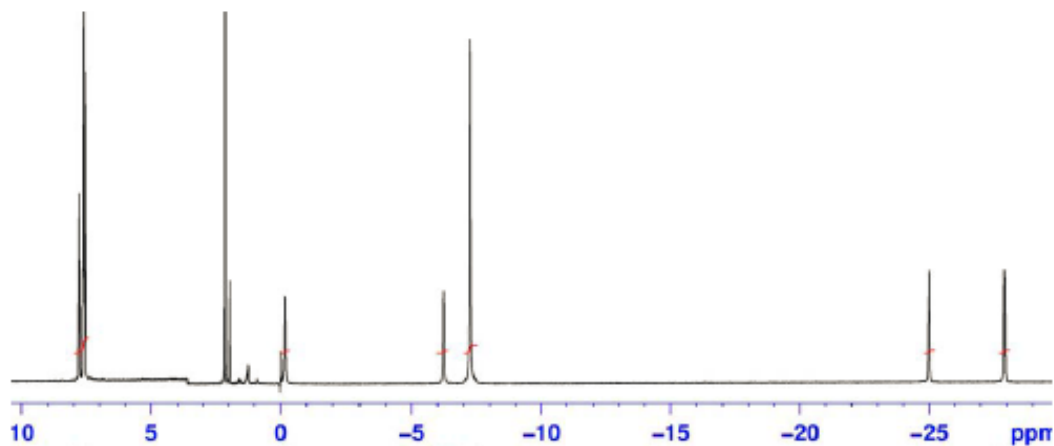


Figure 3. ^1H NMR spectrum of **7b** in CD_3CN . Assignments (δ): -27.9, -25.0, -6.2 and -0.1 (2H, phenylene hydrogens); -7.3 (6H, CH_3); 7.5-8.0 (20H, PPh_4).

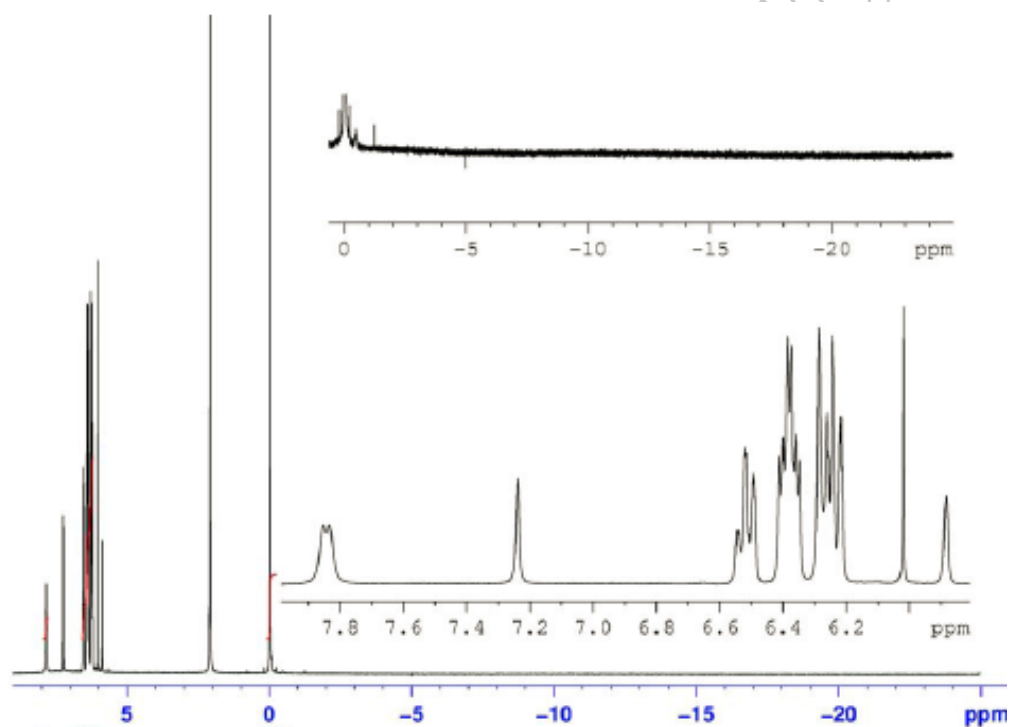


Figure 4. ^1H NMR spectrum of **7b** in CDCl_3 recorded in the excess of d_5 -py. The top inset highlights the absence of resonances at $\delta < 0$; the bottom inset details resonances of aromatic protons.

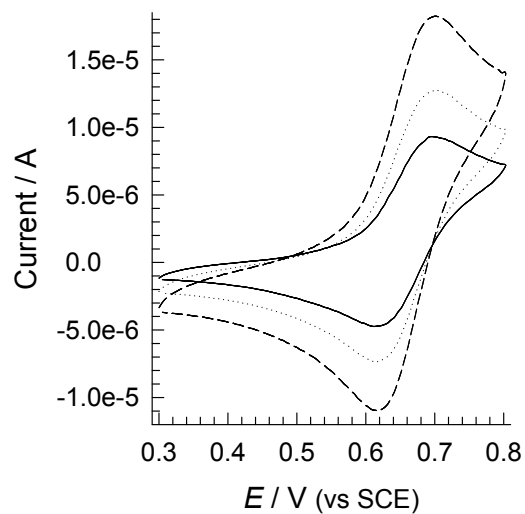


Figure 5. Cyclic voltammograms of **7b** (0.001 M) at a glassy carbon electrode and scan rates 50, 100, and 200 mV s^{-1} in MeCN in the presence of 0.1 M $[\text{nBu}_4\text{N}][\text{PF}_6]$.

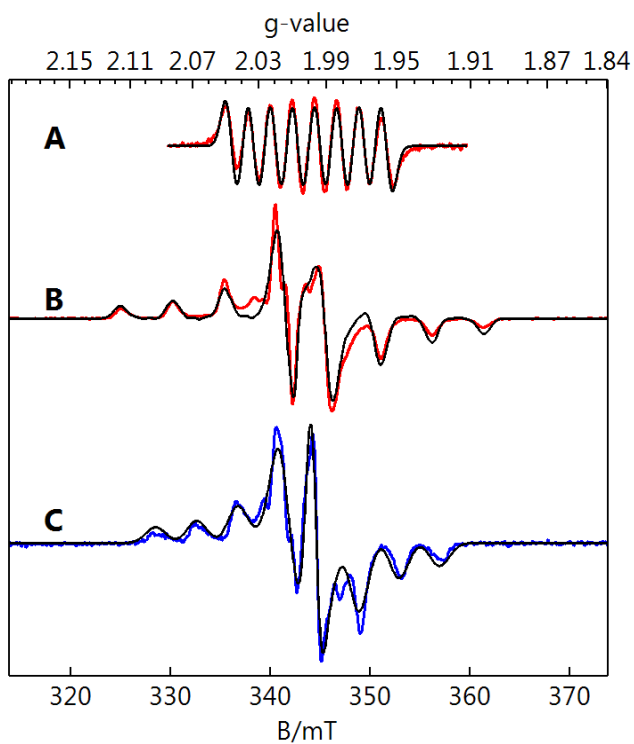


Figure 6. EPR spectra (9.625 GHz) of **14a** (A, B) and **14b** (C) in CH_2Cl_2 . The black traces are simulations (see text for parameters). Sample temperatures 10 K (B, C); 300 K (A).

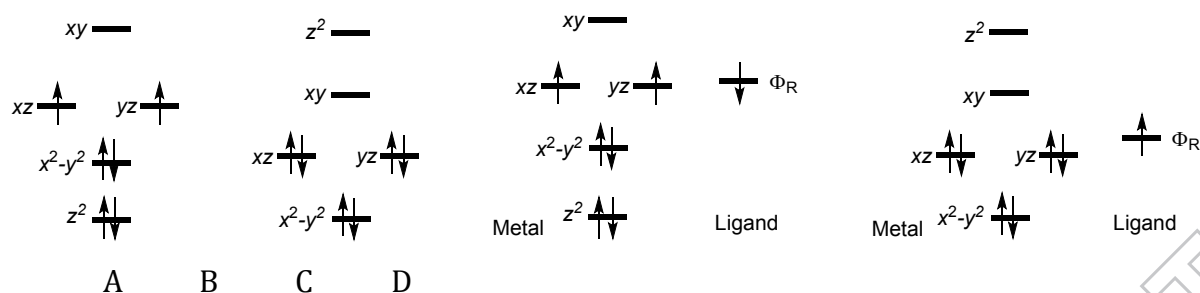


Figure 7. DFT supported *d* orbital diagrams for anionic cobalt(III) TAML complexes **7** ($S = 1$) (A) and **7a** ($S = 0$) (B), neutral (formally Co^{IV}) complexes **13** ($S = \frac{1}{2}$) (C) and **14** ($S = \frac{1}{2}$) (D). Abstracted in part from ref. [40].

Table 1. Comparison of the reduction potentials (vs SCE) for one-electron oxidation of Co^{III} complexes of various TAMLs.

Complex	Solvent	Behavior type	$E_{1/2} / \text{V}$	Reference
1	CH_2Cl_2	a)		[6, 37]
2a	MeCN	Reversible	1.00	[15]
2b ^{b)}	CH_2Cl_2	Reversible	0.98	[9]
2b	CH_2Cl_2	Reversible	0.846	[7]
3b	MeCN	c)		[11]
4	MeCN	Irreversible	0.825	[14]
5	MeCN	Reversible	0.846	[12]
6	MeCN	d)		[13]
7b	MeCN	Reversible	0.66	This work

a) No electrochemical activity up to 2.0 V vs NHE.

b) Variant of **2b** with two $\text{C}(\text{cyclohexyl})_2$ instead of two CMe_2 groups.

c) No electrochemical features reported at potentials above 0.0 V.

d) Only irreversible feature at 1.2 V was reported.

